E-ISSN 2581 – 7957
P-ISSN 2277 – 3916
CVR Journal of Science and Technology, Volume 24, June 2023
DOI: 10.32377/cvrjst2406

Development of Ultrasound Image Detection System based on Chirp-Coded Excitation

C. Pramod Kumar[1] and Narendra. B. Mustare[2]
[1]Sr. Asst. Professor, CVR College of Engineering/ EIE Department, Hyderabad, India
Email: Pramod.kumar@cvr.ac.in
[2]Professor, CVR College of Engineering/ EIE Department, Hyderabad, India
Email: narendra@cvr.ac.in

Abstract: **In addition to enhancing contrast for imaging, high-frequency ultrasound with contrast agents also supports regional genomics research and may be used for medication administration. The possible signal-to-noise ratio (SNR) and depth of penetration of high-frequency ultrasound are important constraints. However, using chirped pulses as trigger signals and a cardinal frequency of 30 MHz, we created a novel ultrasound system in this work that uses chirp-coded-excitation ultrasound imaging. A home-made expander that used a novel peep pulse with contrast agents to reduce pulse compression and energy decay in human tissue improved the signal-to-noise ratio (SNR) by 20dB for high-frequency ultrasound flow imaging of the zebrafish heart, and the penetration depth increased to 2.2mm. Yet, a microbubble experiment that used variable echo signal concentrations was successful in distributing a variety of microbubble types as anticipated. Using the setup that we developed, we can demonstrate experimentally that chirp-encoded excitation reduces the signal-to-noise ratio (SNR) by about 43dB compared to unipolar and bipolar pulse excitation.**

Index Terms: **SNR, High-frequency ultrasound, Chirped pulses, Image detection system, Microbubble**

I. Introduction

Chirp-coded excitation has recently been discovered to offer the potential to increase local medication administration and improve imaging. In the human body, ultrasonic frequency directly correlates to attenuation. The degree of ultrasonic attenuation through tissue increases with ultrasound frequency. As a result of this lessening impact, the ultrasonic energy of a high-recurrence signal is ordinarily lower than that of a low-recurrence signal. Moreover, the signal-to-noise ratio (SNR) and sensitivity of a high-frequency ultrasonic signal are limited because it is more susceptible to interference from internal and external systems. We can raise the SNR of a high-frequency ultrasound imaging system by maintaining a consistent level of system noise. [1]. There are two ways to increase the trigger signal's power. The first strategy is to boost the trigger signal's loudness for greater system sensitivity. In most cases, the maximum mechanical index has already been reached for the pulse amplitude of commercial ultrasound devices (MI). The second technique is to prolong the signal's transmission time to boost the trigger signal's average power. A coded waveform is the name for this processed signal. It is suggested that the coded waveform be used to improve the ultrasound system's SNR and depth of penetration. The pulse duration might, however, be lengthened. Keep in mind that the duration of the sent signal is what ultimately decides the axial resolution. The axial goal of pictures is re-established with the assistance of the trill-coded excitation procedure by changing the normal force of the coded waveform into the immediate force of a short heartbeat, thus expanding the sign plentifulness. In this review, we utilized a peep signal excitation strategy to help the sign strength of the reverberation signal, considering higher spatial goal in the resulting images. The echo signal is then pulse compressed to restore the axial resolution. To compare the properties of the coded waveform with those of a brief pulse, we employ phantoms and wire phantoms. Then, in contrast imaging, the coded excitation is used to improve the picture quality [2].

The SNR and axial resolution of an ultrasound picture is impacted by the chirp-coded excitation method. SNR and penetration depth are both negatively impacted by a brief pulse. Despite this, a brief pulse has a broad bandwidth and a high axial resolution. A longer pulse with more energy has better entrance profundity and SNR, however less hub goal because of its restricted band. One sort of extensive heartbeat is a coded signal. Coded excitation pushes the limits of this compromise by working on the SNR proportion and the infiltration profundity by fitting coding on the communicating part and deciphering on the getting side. Single-communicate codes simply need a solitary succession to be packed by a channel. Conversely, in different send frameworks, compression can only be achieved by combining two or more courses. Biphasic is one of the most often used phase-modulated codes, and the illustrative waveforms are Barker and Golay codes with symbols ± 1.

The swept-frequency chirp is the most prevalent kind of frequency modulation. It is known that the chirp's immediate frequency varies linearly with time [3]. This chirp's pulse is longer than that of other chirps, such as the Gaussian chirp, in the same bandwidth. A longer pulse has more energy. As a result, it is challenging to attenuate such a pulse, which ultimately results in an increase in SNR. Regrettably, the axial resolution is decreased even more due to the overlapping of echo signals caused by a longer pulse. When this is the case, a pressure channel is utilized to abbreviate a long heartbeat into numerous more limited heartbeats to work on the hub goal. The ideal chirp has qualities like; long pulse length and increase in instantaneous frequency of chirps over time [4,5]. As the excitation signal, we choose the chirp whose frequency varies over time. It can precisely match the frequency response of sensors. The next pulse compression enables effective transmission of the trigger

Received on 15-03-2023, Revised on 14-04-2023, Accepted on 25-04-2023.

CVR Journal of Science and Technology, Volume 24, June 2023
DOI: 10.32377/cvrjst2406

signal and the elimination of the nonlinear phase [6]. The arbitrary waveform generator's output seen in figure 1(a).

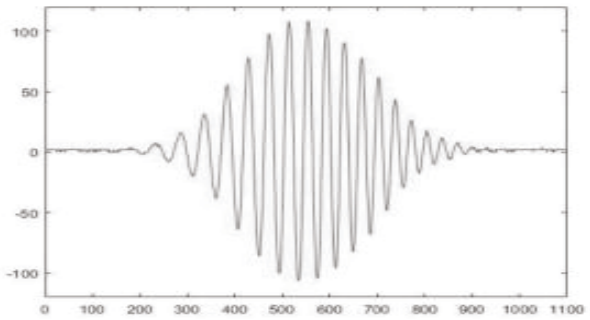

Figure 1(a). Simulated single RF-line data of chirp.

As can be seen in Fig. 1(b), the chirp signals exceeding 100 V are amplified by the power amplifier before being sent as trigger signals to the trigger sensor.

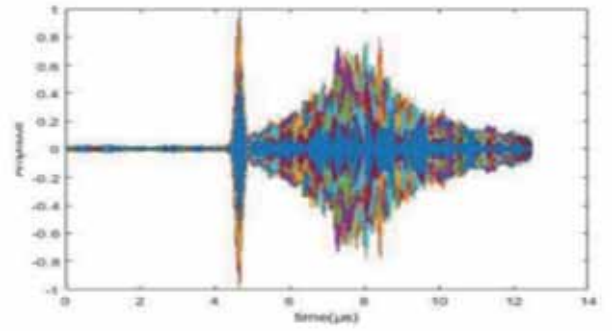

Figure 1(b) . Chirp after amplification with no attenuation.

With the goal of increasing both the average signal intensity,SNR and penetration depth of the proposed framework, we fostered an ultrasonic framework that involves the tweet waveform as the trigger sign. Figure 2 shows a block diagram of the chirp coded-excitation ultrasonic system, demonstrating the various components of the system[7]. These components include the inconsistent waveform generator and the erratic waveform power amplifier.

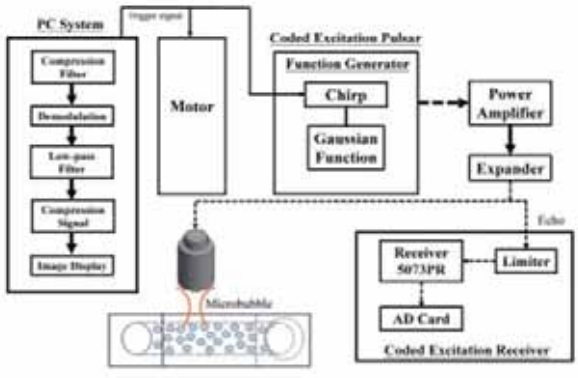

Figure 2.A functional block diagram of a chirp-coded-excitation ultrasound system.

II. METHODOLOGY

A. Coded Excitation Signal

A commercial ultrasonic pulse system's trigger signal is amplified to its maximum MI to enhance the device's efficiency when used in an ultrasound imaging system. Ultrasound produces high instantaneous pressure, which may cause tissue injury through overheating and cavitation effects if not properly mitigated by limiting the transmitted signal energy. The average power of the trigger signal is not relevant for defining short-pulse energy; rather, the power amplitude of the signal is. [8,9]. Chirp-coded excitation may boost SNR and depth of penetration by increasing the signal's average energy without changing the loudness of the trigger signal [10].

A shorter pulse has a smaller bandwidth envelope in the spectrum than a longer one. Because of this, the axial resolution would not be recovered from a long-pulse echo using a compression filter. Using a chirp as a carrier, we were able to get the bandwidth of a long pulse down to the same level as a short pulse in this study. Since that chirp frequency grows with time, its bandwidth is much larger than that of a constant-frequency sine wave carrier. When a lengthy pulse is carried by a chirp, the bandwidth is increased, and the echo is compressed [11]. A chirp is described as

$$c(t) = w(t)\cos\left[2\pi\left(f_0 - \frac{\Delta f}{2}t + \alpha t^2\right)\right], 0 \le t \le T, \qquad (1)$$

At some time in the future, where w(t) is a window of Gaussian distribution, f_o is the carrier frequency, f is the bandwidth, T is the signal length and frequency increment rate (=2f/T). The compression ratio function controls how long the chirp signal is played. A Gaussian pulse is the product of a chirp signal with a Gaussian envelope. Altering the chirp duration of a Gaussian chirp pulse yields signals of varying lengths while maintaining consistent bandwidths [12].

B. System Descriptions

An ultrasonic transducer with a 30 MHz central frequency and a 6 mm element diameter was used in this investigation.Fig.3(a) shows a typical acquired echo waveform.

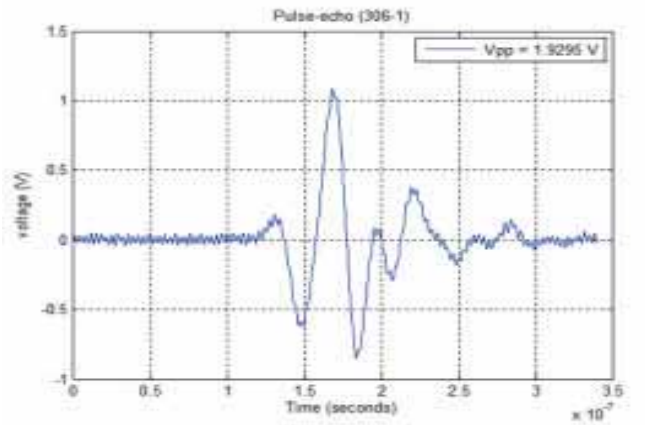

Figure 3. (a) Waveform of a pulse echo

As we can see in Fig.3(a), the transducer generates a signal of 1.92V peak to peak and with a delay of 1.4 microseconds, and frequency of 30 million cycles per second [13]. Higher frequencies generally provide better resolution and are suitable for imaging shallow structures or

fine details. The emitted pulse is having a pulse duration of about 0.7 microsecond which improves axial resolution to distinguish between closely spaced reflectors along the path of the ultrasound beam. We can also see the leading edge of the echo is having a rapid rise time that allows for accurate determination of the time of flight for the ultrasound pulse, which is used to calculate the distance to the target.

Fig.3(b) explains the frequency response of the ultrasound transducer that we are using in our experiment. For an ultrasound transducer with a centre frequency of 30 MHz, the frequency response is typically like a bell-shaped curve centred around 30 MHz. The exact shape and width of the curve will depend on various factors, including the design of the transducer, the materials used, and the application for which it is intended [14]. The width of the frequency response curve, often referred to as the bandwidth, is relatively narrow, typically ranging from a few megahertz below to a few megahertz above the center frequency.

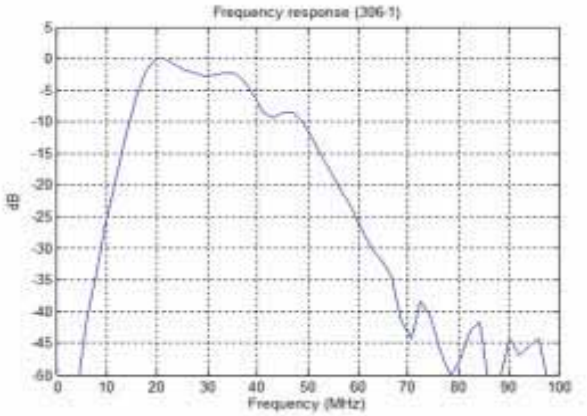

Figure 3. (b) Frequency Response

Both the transducer and the brass enclosure are coated with a protective parylene-c layer, which also serves as a matching layer. Transmission efficiency and ultrasonic reflectivity back to the sensor are both improved by adding this layer [15].

Both a function generator operating at 240 MHz sample/s and an arbitrary waveform power amplifier were part of the pulse system. The arbitrary waveform generator takes its input from computer-generated waveforms that are sent by the spatial programming. The AWG may subsequently give an extensive variety of helpful transmission signals. The increase of a 325LA is ostensibly 50 dB, with a gain fluctuation of 1.5 dB at most. In addition, the frequency response of the input voltages of the 325LA is flat from 250 kHz to 125 MHz input voltages over the peak voltage may cause irreparable harm to the instrument. A 5073PR ultrasonic receiver is used in this research, with a maximum bandwidth of 1 kHz to 75 MHz. There is a 7 V peak-to-peak spread in the receiver's noise floor. As the function generator's trigger signal input, the MATLAB-edited chirp waveform is amplified by the power amplifier to produce a high-voltage pulse. The trigger signal is expanded by a diode circuit (expander) to remove noise; this is necessary because the power amplifier amplifies any noise that may be present in the trigger signal; finally, the trigger signal activates the high-frequency transducer, which sends out the ultrasound signal [16]. To shield the receiver's sensitive electronics from the high-voltage trigger signal, the reflected signal is routed via a second diode circuit (limiter) before it reaches the receiver. When the echo signal has been picked up, the 5073 PR receiver will boost it to the correct levels. After that, signal processing is used to convert the echo signal into visuals. A transducer for imaging scanning is mounted in the stationary section, and motion is generated in all three dimensions. The x-axis is steered by an HR8 ceramic linear servo motor, the main scan control motor. Both the y- and z-axis movements are controlled by high-precision stepper motors. The position may be fixed in space in all three dimensions thanks to the three-dimensional motion system. Specifications of the three-dimensional motion system are shown in Table 1.

TABLE I.
THREE-DIMENSIONAL MOTION SYSTEM'S SPECIFICATIONS.

Axis	Stroke (mm)	Count (µm)	Load (kg)	Velocity (mm/s)
x	150	0.1	2	150
y	300	0.8	10	100
z	50	0.6	2	50

C. Signal Processing

There are two distinct components to ultrasound signal processing and imaging. In the first, the echo signal is compressed to reduce its phase difference and concentrate its energy to restore its axial resolution. This study's compression filter of choice is a matched filter. An optimum ultrasonic signal is applied with the matching filter. Hence, pulse compression is accomplished by concentrating the echo signal's energy. Demodulation makes up the second phase. Using an ultrasonic transducer, the echo signal is demodulated to filter the carrier and diversify the wave crest. To create B-mode pictures, the compressed signal will next be converted. The trigger signal for the ultrasound system's imaging scans is produced by an arbitrary waveform generator. To activate the transducer to generate an ultrasonic signal, the trigger signal is amplified using an arbitrary waveform amplifier. The receiver picks up the echo signal, suitably amplifies it, and then feeds it to the oscilloscope for visual display. The experimental system is presented using a test block diagram. Oscilloscope results from the system test demonstrate that it is challenging to see the echo signal when it is obscured by noise. To identify and eliminate the noise source, each instrument's output signal is analysed. To increase the SNR, the right receiver is selected.

Schottky diodes are used in a traditional radar and ultrasound system to reduce nonlinear noise, improving the system SNR and spatial resolution at the same time. Expanders are produced using standard Schottky diodes, such as 1N4148 and 1N914. A trigger signal (30 MHz) is used to set the echo signal to 0.5 V chirp, and the echo signal's SNR is then measured. Three different kinds of expanders are related to the power amplifier. Table 2

CVR Journal of Science and Technology, Volume 24, June 2023
DOI: 10.32377/cvrjst2406

displays the calculated findings. Expanders may lessen the power amplifier's noise in both commercial and homemade fashion. To effectively increase the SNR of the echo signal, the sound is reduced to 0.04 V. In this investigation, expander 1N4148 will be utilised to minimise noise since its SNR for the echo signal is superior to that of the other expanders.

TABLE II.
ECHO SIGNAL MEASUREMENTS WITH VARIOUS EXPANDER

Measured Results	1N4148 Expander	Commercial Expander	Handmade Expander
Peak Voltage	1.42 V	1.38 V	1.38 V
Noise Voltage	0.04 V	0.04 V	0.04 V
SNR	31dB	30.75 dB	30.75 dB

D. Microbubble Imaging

A discussion of microbubble concentration is essential when using them. The scatter signal will be insufficient to improve picture contrast if the microbubble concentration is too low. Interestingly, if the microbubble focus is too high, the ultrasonic sign will be a lot more fragile, and it won't be possible to picture the object's back. The shielding effect refers to this. Thus, it is necessary to determine the proper microbubble concentration. The selection of the proper microbubble concentration is crucial given that microbubbles will also be employed for in vitro research. Little animals' blood circulation will dilute microbubbles administered to them, decreasing the scatter signal's strength. Nevertheless, thrombosis will happen if tiny animals get an excessive number of microbubbles by injection. So, the microbubbles may keep their enormous scattering capability and not cause thrombosis if they are at a concentration that can be diluted by an animal's blood circulation. The microbubble sizes employed in this research are C3F8 1.1 m, C3F8 2 m, C4F10 1.1 m, and C4F10 2 m.

Suppose that the blood circulation will eventually dilute the microbubbles put into a tiny animal. The concentration of microbubbles drops by 10–100% in stages of 10%. The ultrasonic scanner receives the injection of the diluted microbubbles into an acrylic phantom. The photos are scanned with a Terason model T3000 from Teratech Company in the United States. The suitable concentration ranges for four distinct kinds of microbubbles are discovered based on the brightness of photographs with various microbubble concentrations. To improve the signal of the blood zone and identify micro perfusion, ultrasound contrast ants are intravenously administered into the bloodstream. Information on the characteristics of microbubble destruction and the distribution of size of microbubbles following disintegration is crucial for medication release. The visual contrast increases as the signal frequency approaches the resonant frequency. The microbubble size must be smaller than 1 m, which is uncommon since the trigger capability in the peep coded-excitation ultrasound framework has a high recurrence. As a result, little microbubbles continue to exist and improve the contrast of the picture while giant microbubbles are eliminated. Three acoustic pressures (0.2, 0.4, and 0.6 MPa) and three signal cycles make up the characteristics of the destruction signal (100, 500, and 1000 cycles). On the ultrasound scan, microbubbles do not continue to be of the same size. With the transition of positive or negative voltage, microbubbles expand or compress, accordingly. As a result, various acoustic pressures are established to track the size distribution of destroyed microbubbles. Indicator cycles influence the time at which microbubbles oscillate. Whenever a certain threshold is reached in the number of signal cycles, a microbubble will break apart into multiple smaller microbubbles. The quantity of microbubbles will then rise as their size declines. To track variations in the quantity of microbubbles, various signal cycle counts are specified. Injection of the microbubbles into an acrylic phantom. The parameters are utilised to produce a destruction signal using the function generator. To create the signal that kills microbubbles, the signal is fed to a 1 MHz transducer (model V303, Panametrics, Waltham, MA) after passing via a power amplifier to amplify it. 1 Hz is the pulse repetition frequency (PRF), and 30 s is the destruction time.

III. EXPERIMENTAL RESULTS

A. Image Phantom Fabrication

Imaging phantom, or simply phantom, is a specially designed object that is scanned or imaged in the field of medical imaging to evaluate, analyze, and tune the performance of various imaging devices. A phantom is more readily available and provides more consistent results than the use of a living subject or cadaver, and likewise avoids subjecting a living subject to direct risk. In electrical engineering, a wire phantom is an electrical circuit derived from suitably arranged wires with one or more conductive paths being a circuit and at the same time acting as one conductor of another circuit. Ultrasound imaging studies might benefit from using the wire phantom as a reference phantom for analysing axial and lateral resolutions, system noise, and dynamic range. To assess the picture resolution, a wire phantom made up of five tungsten wires with a diameter of 20 m is employed. With axial and lateral spacing's of 1 and 2 mm, respectively, the cables are diagonally aligned. As a result, the efficacies of scanning pictures with unipolar pulse, bipolar pulse, and chirp-coded excitations are compared. Images of wire phantoms with various excitations are shown in Figure 4.

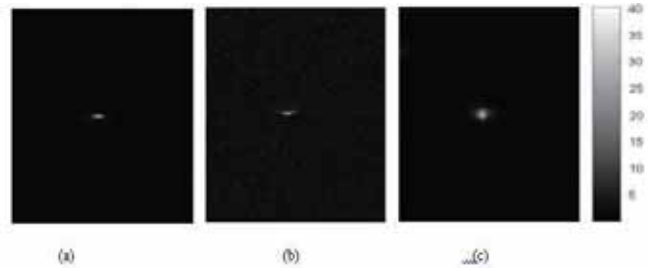

Figure 4. Pictures of a wire phantom:(a) Imaging with unipolar pulses (b) Imaging using bipolar pulses (c) Imaging using chirp-coded excitation

The size of the resonation signal from the wire around the middle point for brief vibration and trill coded excitation is shown in Figure 5. SNRs for short pulses and coded excitation are 31 dB and 43 dB, respectively. Hence, the

CVR Journal of Science and Technology, Volume 24, June 2023
DOI: 10.32377/cvrjst2406

SNR of the proposed system increased to 12 dB in the case of chirp-coded excitation in compared to the SNR of the commercial ultrasonic pulse system.

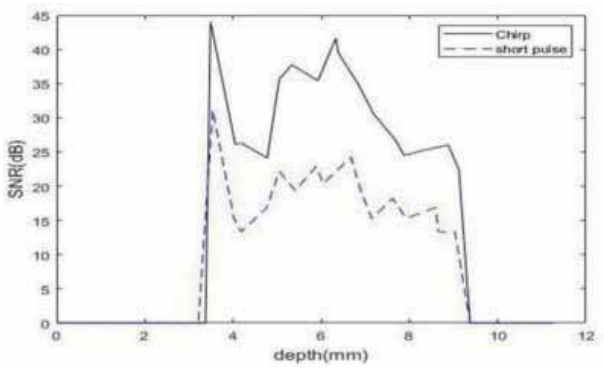

Figure 5.SNR for chirp-coded and short pulse excitation as a function of depth

The wire of the wire phantom should look circular in the photos; however, this is not the case since the cable is out of the focus point, causing distortion in the wire images. To indicate the degree of deformation in a certain point as a function of depth, the deformed wire pictures' minor axis to major axis ratio is a parameter. Increases in deformation cause a corresponding increase in the distance between the wire and the focal point. A brief pulse causes more deformation than coded excitation does, which is more severe. The findings were contrasted with an ultrasound picture for a different sort of stimulation. Hence, a soft tissue phantom (8 cm long, 5 cm wide, and 1.5 cm high) was employed to imitate the actual circumstances in which the ultrasound would be delivered. To scan the tissue phantom, a brief pulse with a trigger signal (30 MHz) and chirp-coded excitation were utilised. The tissue phantom pictures acquired using various forms of coded excitation are shown in Figure 6. As a result of the coded stimulation, the penetration depth increased to two mm, as compared to the unipolar pulse excitation.

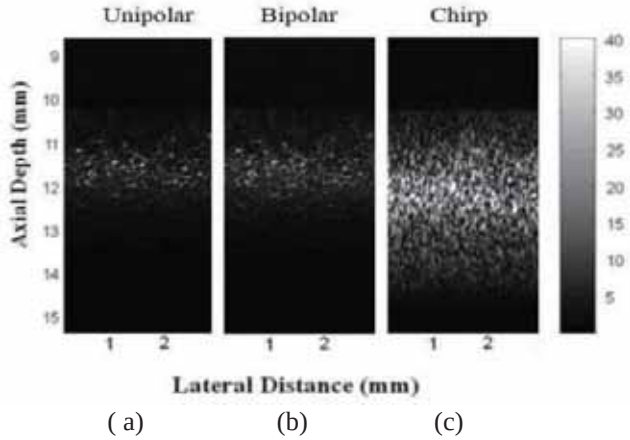

Figure 6. Ultrasound phantom images (a) Excitation of unipolar pulses (b) Excitation of a bipolar pulse (c) Excitation using chirp-codes.

B.. Microbubble imaging

In this study, four different kinds of microbubbles were employed. Choosing the right concentration range avoids the microbubble concentration from being too high, which would significantly attenuate the ultrasonic signal, or too low, which would improve the picture contrast. As a result, ten concentrations of the four different kinds of microbubbles are created.

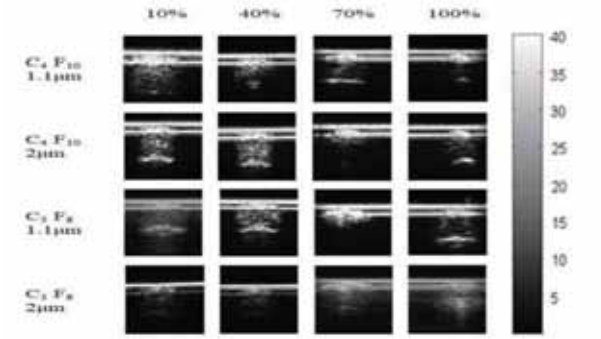

Figure 7. Contrast images for four microbubble concentrations: C3F8 1.1 μm, C3F8 2 μm, C4F10 1.1 μm, and C4F10 2 μm.

Figure 7 above displays contrast pictures of four distinct kinds of microbubbles at various intensities. The ultrasonic chirp coded-excitation system is activated by a radio frequency signal. The visual contrast is much stronger when the signal frequency is nearer to the resonance frequency of microbubbles. Yet, the relationship between the resonant frequency and the size of the microbubbles is inverse. The resonance frequency rises as the microbubble size decreases. In contrast, the resonance frequency decreases as the size of the microbubbles increases. Lately, the zebrafish heart has emerged as a potent model for comprehending the capacity for self-healing, making the zebrafish an essential component of regenerative medicine. As a result, microbubbles are employed to improve the visual contrast while observing zebrafish. Figure 8 shows a comparison of the zebrafish heart before and after microbubble injection.

Figure 8(a) depicts the zebrafish heart without microbubbles; all that can be seen is the shape of the breast. The zebrafish heart is seen in Figure 8(b) after microbubble injection. The heart's atrium and ventricle are visible.

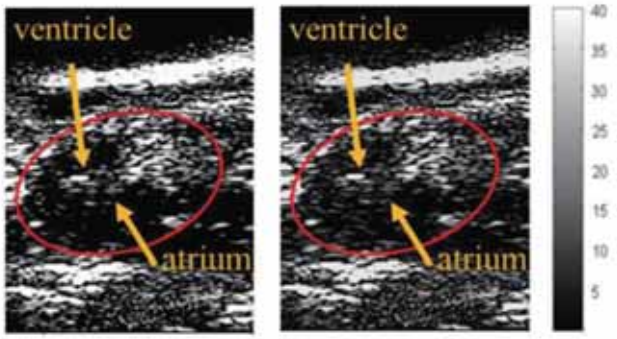

Figure 8. (a) Zebrafish heart devoid of microbubbles. (b) Zebrafish heart after injection of microbubbles

IV. Conclusions

In this work, we assessed how well the high-frequency ultrasonic detection method performed when contrast chemicals were used. Hence, we were able to demonstrate numerically and subjectively that chirp-coded excitation results in an SNR enhancement of roughly 12 dB over short-pulse excitation when employing the proper receiver and homemade expander. Nevertheless, in the view, injection of four different kinds of microbubbles revealed the following suitable concentration ranges from the microbubble imaging experiment.: C3F8, 1.1 μm from 20 to 40%; C3F8, 2 μm from 80 to 100%; C4F10, 1.1 μm from 20 to 40%; and C4F10, 2 μm from 30 to 50%. The dispersion of microbubble sizes shrank with the precise setting of the destruction signal. Hence, the image contrast is enhanced when the signal frequency is close to the resonance frequency of the microbubbles. The microbubbles were injected into zebrafish, and the fish were then subjected to an ultrasound examination utilising a chirp-coded-excitation system to detect and analyse cardiac alterations before and after the microbubble injection. An excitation-coded ultrasound system using microbubbles could one day be used to examine tumours in small animals without the need for necropsy. Since chirps have more energy and may thus achieve greater penetration and SNR, they may potentially be utilised as carriers for medications that are burst to release them at a specified location.

References

[1] Chaturvedi P., Insana M.F., Hall T.J. 2-D companding for noise reduction in strain imaging. IEEE Trans. Ultrason. Ferroelectr. Freq. Control. 1998;45:179–191. doi: 10.1109/58.646923. [PubMed] [CrossRef] [Google Scholar]

[2] Behar V, Adam D. Parameter optimization of pulse compression in ultrasound imaging systems with coded excitation. Ultrasonics. 2004;vol. 42:1101–1109. [PubMed] [Google Scholar]

[3] Peng H., Liu D.C. Chirp-coded pulse excitation for ultrasound elasticity imaging; Proceedings of the 2010 4th International Conference on Bioinformatics and Biomedical Engineering (iCBBE); Chengdu, China. 18–20 June 2010; pp. 1–4. [Google Scholar]

[4] O'Donnell M. Coded excitation system for improving the penetration of real-time phased-array imaging systems. IEEE Trans. Ultrason. Ferroelectr. Freq. Control. 1992;39:341–351. doi: 10.1109/58.143168. [PubMed] [CrossRef] [Google Scholar]

[5] Chiao RY, Hao X. Coded excitation for diagnostic ultrasound: a system developer's perspective. IEEE Trans Ultrason Ferroelectr Freq Control. 2005;vol. 52:160–170. [PubMed] [Google Scholar]

[6] Gennisson J.L., Deffieux T., Fink M., Tanter M. Ultrasound elastography: Principles and techniques. Diagn. Interv. Imaging. 2013;94:487–495. doi: 10.1016/j.diii.2013.01.022. [PubMed] [CrossRef] [Google Scholar]

[7] Liu J., Insana M.F. Coded pulse excitation for ultrasonic strain imaging. IEEE Trans. Ultrason. Ferroelectr. Freq. Control. 2005;52:231–240. [PMC free article] [PubMed] [Google Scholar]

[8] Peng H., Liu D.C. Enhanced ultrasound strain imaging using chirp-coded pulse excitation. Biomed. Signal Process. Control. 2013;8:130–141. doi: 10.1016/j.bspc.2012.09.002. [CrossRef] [Google Scholar]

[9] Qiu W., Yu Y., Tsang F.K., Zheng H., Sun L. A novel modulated excitation imaging system for microultrasound. IEEE Trans. Biomed. Eng. 2013;60:1884–1890. [PubMed] [Google Scholar]

[10] C. Yoon, W. Lee, J. H. Chang, T.-K. Song, and Y. Yoo, "An efficient pulse compression method of chirp-coded excitation in medical ultrasound imaging," IEEE Trans. Ultrason., Ferroelect., Freq. Control, vol. 60, no. 10, pp. 2225–2229, Oct. 2013.

[11] P. Song, M. W. Urban, A. Manduca, J. F. Greenleaf, and S. Chen, "Coded excitation plane wave imaging for shear wave motion detection," IEEE Trans. Ultrason., Ferroelect., Freq. Control, vol. 62, no. 7, pp. 1356–1372, Jul. 2015.

[12] J. Song, J. H. Chang, T.-K. Song, and Y. Yoo, "Coded tissue harmonic imaging with nonlinear chirp signals," Ultrasonics, vol. 51, no. 4, pp. 516–521, May 2011

[13] J.-M. Girault, F. Ossant, A. Ouahabi, D. Kouame, and F. Patat, "Timevarying autoregressive spectral estimation for ultrasound attenuation in tissue characterization," IEEE Trans. Ultrason., Ferroelect., Freq. Control, vol. 45, no. 3, pp. 650–659, May 1998.

[14] Y. B. Ahn and S. B. Park, "Estimation of mean frequency and variance of ultrasonic Doppler signal by using second-order autoregressive model," IEEE Trans. Ultrason., Ferroelect., Freq. Control, vol. 38, no. 3, pp. 172–182, May 1991.

[15] Bae B, Lee H, Lee S, Lee W, Roh Y. Development of a highly attenuative backing for ultrasonic transduces with periodic arrangement of polymeric rods inside the backing. In: Conference proceedings of the IEEE ultrasonic symposium; 2013. p. 1105–08.

[16] P. Zhu, H. Peng, L. Mao, and J. Tian, "Piezoelectric single crystal ultrasonic transducer for endoscopic drug release in gastric mucosa," IEEE Transactions on Ultrasonics, Ferroelectrics, and Frequency Control, vol. 68, no. 4, pp. 952–960, 2021